CLEO-CONF 03-08
LP-279

Measurement of the Hadronic Recoil Mass Moments in Semileptonic B Decay*

G. S. Huang,[1] D. H. Miller,[1] V. Pavlunin,[1] B. Sanghi,[1] E. I. Shibata,[1] I. P. J. Shipsey,[1] G. S. Adams,[2] M. Chasse,[2] J. P. Cummings,[2] I. Danko,[2] J. Napolitano,[2] D. Cronin-Hennessy,[3] C. S. Park,[3] W. Park,[3] J. B. Thayer,[3] E. H. Thorndike,[3] T. E. Coan,[4] Y. S. Gao,[4] F. Liu,[4] R. Stroynowski,[4] M. Artuso,[5] C. Boulahouache,[5] S. Blusk,[5] E. Dambasuren,[5] O. Dorjkhaidav,[5] R. Mountain,[5] H. Muramatsu,[5] R. Nandakumar,[5] T. Skwarnicki,[5] S. Stone,[5] J.C. Wang,[5] A. H. Mahmood,[6] S. E. Csorna,[7] G. Bonvicini,[8] D. Cinabro,[8] M. Dubrovin,[8] A. Bornheim,[9] E. Lipeles,[9] S. P. Pappas,[9] A. Shapiro,[9] W. M. Sun,[9] A. J. Weinstein,[9] R. A. Briere,[10] G. P. Chen,[10] T. Ferguson,[10] G. Tatishvili,[10] H. Vogel,[10] M. E. Watkins,[10] N. E. Adam,[11] J. P. Alexander,[11] K. Berkelman,[11] V. Boisvert,[11] D. G. Cassel,[11] J. E. Duboscq,[11] K. M. Ecklund,[11] R. Ehrlich,[11] R. S. Galik,[11] L. Gibbons,[11] B. Gittelman,[11] S. W. Gray,[11] D. L. Hartill,[11] B. K. Heltsley,[11] L. Hsu,[11] C. D. Jones,[11] J. Kandaswamy,[11] D. L. Kreinick,[11] V. E. Kuznetsov,[11] A. Magerkurth,[11] H. Mahlke-Krüger,[11] T. O. Meyer,[11] N. B. Mistry,[11] J. R. Patterson,[11] T. K. Pedlar,[11] D. Peterson,[11] J. Pivarski,[11] S. J. Richichi,[11] D. Riley,[11] A. J. Sadoff,[11] H. Schwarthoff,[11] M. R. Shepherd,[11] J. G. Thayer,[11] D. Urner,[11] T. Wilksen,[11] A. Warburton,[11] M. Weinberger,[11] S. B. Athar,[12] P. Avery,[12] L. Breva-Newell,[12] V. Potlia,[12] H. Stoeck,[12] J. Yelton,[12] B. I. Eisenstein,[13] G. D. Gollin,[13] I. Karliner,[13] N. Lowrey,[13] C. Plager,[13] C. Sedlack,[13] M. Selen,[13] J. J. Thaler,[13] J. Williams,[13] K. W. Edwards,[14] D. Besson,[15] K. Y. Gao,[16] D. T. Gong,[16] Y. Kubota,[16] S. Z. Li,[16] R. Poling,[16] A. W. Scott,[16] A. Smith,[16] C. J. Stepaniak,[16] J. Urheim,[16] Z. Metreveli,[17] K.K. Seth,[17] A. Tomaradze,[17] P. Zweber,[17] J. Ernst,[18] H. Severini,[19] P. Skubic,[19] S. A. Dytman,[20] J. A. Mueller,[20] S. Nam,[20] and V. Savinov[20]

(CLEO Collaboration)

[1]Purdue University, West Lafayette, Indiana 47907
[2]Rensselaer Polytechnic Institute, Troy, New York 12180
[3]University of Rochester, Rochester, New York 14627
[4]Southern Methodist University, Dallas, Texas 75275
[5]Syracuse University, Syracuse, New York 13244
[6]University of Texas - Pan American, Edinburg, Texas 78539
[7]Vanderbilt University, Nashville, Tennessee 37235
[8]Wayne State University, Detroit, Michigan 48202
[9]California Institute of Technology, Pasadena, California 91125
[10]Carnegie Mellon University, Pittsburgh, Pennsylvania 15213
[11]Cornell University, Ithaca, New York 14853
[12]University of Florida, Gainesville, Florida 32611
[13]University of Illinois, Urbana-Champaign, Illinois 61801
[14]Carleton University, Ottawa, Ontario, Canada K1S 5B6
and the Institute of Particle Physics, Canada
[15]University of Kansas, Lawrence, Kansas 66045
[16]University of Minnesota, Minneapolis, Minnesota 55455
[17]Northwestern University, Evanston, Illinois 60208
[18]State University of New York at Albany, Albany, New York 12222

[19]*University of Oklahoma, Norman, Oklahoma 73019*
[20]*University of Pittsburgh, Pittsburgh, Pennsylvania 15260*
(Dated: July 29, 2003)

Abstract

We present a preliminary measurement of the composition of inclusive semileptonic B meson decays using 9.4 fb^{-1} of e^+e^- data taken with the CLEO detector at the $\Upsilon(4S)$ resonance. In addition to measuring the charged lepton kinematics, the neutrino 4-vector is inferred using the hermiticity of the detector. We perform a maximum likelihood fit over the full three-dimensional differential decay distribution for the fractional contributions from the $B \to X_c l\nu$ processes with $X_c = D$, D^*, D^{**}, and nonresonant X_c, and the process $B \to X_u l\nu$. From the fit results we extract $\langle M_X^2 - \overline{M}_D^2 \rangle = (0.456 \pm 0.014 \pm 0.045 \pm 0.109)$ GeV$^2/c^4$ with minimum lepton energy of 1.0 GeV and $\langle M_X^2 - \overline{M}_D^2 \rangle = (0.293 \pm 0.012 \pm 0.033 \pm 0.048)$ GeV$^2/c^4$ with minimum lepton energy of 1.5 GeV. The uncertainties are from statistics, detector systematic effects, and model dependence, respectively.

*Submitted to XXI International Symposium on Lepton and Photon Interactions at High Energies, August 11-16, 2003, Fermi National Accelerator Laboratory, Batavia, IL.

I. INTRODUCTION

Nonperturbative QCD physics connects measurements of B meson decay properties to the properties of underlying weak flavor changing currents. Heavy-quark effective theory (HQET) combined with the operator product expansion (OPE) provides a framework in which many inclusive B decay properties can be calculated [1].

Using HQET, the inclusive B decay matrix elements can be expanded in powers of Λ_{QCD}/M_B. For each order in the expansion new nonperturbative parameters arise. At order Λ_{QCD}/M_B, there is $\overline{\Lambda}$and at order Λ^2_{QCD}/M^2_B, there are λ_1 and λ_2. The nonperturbative parameter $\overline{\Lambda}$ relates the b-quark mass to the B meson mass in the limit of infinite b-quark mass. The parameter λ_2 is directly related to the mass splitting between the B^* and B mesons. Moments of kinematic variables can be used to determine the $\overline{\Lambda}$ and λ_1 parameters. These parameters are properties of the B meson and are not specific to the decay mode being studied. This means that moments of the lepton energy and the X_c mass in $B \to X_c l\nu$ decays can be related to moments of the photon energy spectrum in $B \to X_s\gamma$. Furthermore, measurements of these parameters can be used in the calculation of absolute decay rates, providing an improved relationship between the $B \to X_c l\nu$ branching fraction and $|V_{cb}|$.

This paper presents a measurement of the first moment of the square of the hadronic mass in $B \to X_c l\nu$ decays as a function of the lepton energy cut. Because the background from secondary leptons becomes large at low lepton energy, the lowest lepton energy considered is 1.0 GeV. Moments of the square of the hadronic mass have previously been measured by CLEO with a lepton energy cut of 1.5 GeV [2] and by BaBar with a lepton energy cut of 0.9 GeV [3]. As the lepton energy cut is made more restrictive, the terms that are higher order in Λ_{QCD}/M_B become more important, making the expansion less reliable [5]. There are significant complications in reducing the minimum lepton energy to 1.0 GeV. The backgrounds from continuum $e^+e^- \to q\overline{q}$ events, fake leptons and secondaries all become more important. The structure of the nonresonant $B \to X_c l\nu$ decays also becomes more important.

In order to reconstruct the recoiling hadronic invariant mass, it is necessary to reconstruct both the charged lepton and neutrino kinematics. The neutrino is reconstructed using the approximate hermiticity of the CLEO II and CLEO II.V detectors [6] and the well known initial state of the e^+e^- system produced by the Cornell Electron Storage Ring (CESR) [4]. The experimental resolution on the neutrino energy has a narrow core with a full width at half maximum height of approximately 120 MeV and a broad tail of over estimation of the neutrino energy which extends up to 1.5 GeV. The square of the hadronic recoil mass, M_X^2, can be calculated if the B momentum, $\vec{p}_B$, is known,

$$M_X^2 \;=\; M_B^2 + q^2 - 2E_{beam}(E_\ell + E_\nu) + 2|\vec{p}_B||\vec{p}_\ell + \vec{p}_\nu|\cos\theta_{B\cdot\ell\nu},$$

where $\theta_{B\cdot\ell\nu}$ is the angle between the momentum of the leptonic system, $\vec{q} = \vec{p}_\ell + \vec{p}_\nu$, and $\vec{p}_B$. Since the B mesons are the daughters of an $\Upsilon(4S)$ produced at rest, the magnitude of the B momentum is known and small, however its direction is unmeasured. The last term in the M_X^2 equation depends on the unknown B momentum direction, but it is small, and therefore neglected in this analysis. Because of the neglected term, the M_X^2 resolution depends on $|\vec{q}|$. The kinematic variables $q^2 = (p_\ell + p_\nu)^2$ and the pseudo-helicity angle of the virtual W, $\cos\theta_{W\ell}$, can also be calculated. The pseudo-helicity angle, $\cos\theta_{W\ell}$, is defined as the cosine of the angle between the lepton momentum in the virtual-W frame and the virtual-W momentum in the lab frame.

From the sample of events with a charged lepton and reconstructed neutrino, the differential decay rate is measured as a function of the reconstructed quantities q^2, M_X^2, and $\cos\theta_{W\ell}$. We fit the observed three-dimensional distribution to a sum of Monte Carlo models for the different hadronic final states: D, D^*, D^{**}, X_c nonresonant, and X_u. The models are constructed with Monte Carlo events generated with a full detector simulation [7] and have the same reconstruction cuts applied as the data. In addition to the $B \to X l\nu$ processes, there are backgrounds from fake leptons, continuum leptons and secondary leptons. The q^2 and $\cos\theta_{W\ell}$ variables add information which contributes to the separation of the signal from the backgrounds, and the separation of the D and D^* final states. The moment $\langle M_X^2 - \overline{M}_D^2\rangle$ is calculated from the fit results for the final states containing charm using the same theoretical models as are used in the fit, but without any detector simulation.

II. DATA SAMPLE AND EVENT SELECTION

The data used in this analysis were taken with two configurations of the CLEO detector, CLEO II and CLEO II.V. An integrated luminosity of 9.4 fb^{-1} was accumulated on the $\Upsilon(4S)$ resonance, $E_{cm} \approx 10.58$ GeV and an additional 4.5 fb^{-1} was accumulated at 60 MeV below the $\Upsilon(4S)$ resonance, where there is no $B\overline{B}$ production. Both detector configurations covered 95% of the 4π solid angle with drift chambers and a cesium iodide calorimeter. Particle identification was provided by muon chambers with measurements made at 3, 5, and 7 hadronic interaction lengths, a time of flight system and specific ionization (dE/dx) from the drift chamber. In the CLEO II configuration, there were three concentric drift chambers filled with a mixture of argon and ethane. In the CLEO II.V detector, the innermost tracking chamber was replaced with a three-layer silicon detector and the main drift chamber gas was changed to a mixture of helium and propane.

Events are selected to have an identified electron or muon with momentum greater than 1 GeV/c and a well reconstructed neutrino. Additional criteria are used to suppress background events from the $e^+e^- \to q\overline{q}$ continuum under the $\Upsilon(4S)$ resonance.

The identified leptons are required to fall within the barrel region of the detector ($|\cos\theta| < 0.71$, where θ is the angle between the lepton momentum and the beam axis). Electrons are identified with a likelihood-based discriminator which combines dE/dx, time of flight, and the ratio of the energy deposited in the calorimeter to the momentum of the associated charged track (E/p). Muons are identified by their penetration into the muon chambers. For momenta between 1.0 and 1.5 GeV/c, muon candidates are required to penetrate at least 3 interaction lengths and above 1.5 GeV/c, candidates are required to penetrate at least 5 interaction lengths. The absolute lepton identification efficiencies are calculated by embedding raw data from reconstructed leptons in radiative QED events into hadronic events. The rate at which pions and kaons fake leptons is measured by reconstructing $K_S^0 \to \pi^+\pi^-$, $D^0 \to K^-\pi^+$, and $\overline{D^0} \to K^+\pi^-$ using only kinematics and then checking the daughter particle lepton identification information.

Neutrinos are reconstructed by subtracting the sum of the four-momenta of all observed tracks and showers not associated with tracks, $p^\mu_{observed}$, from the four-momentum of the e^+e^- initial state, $p^\mu_{e^+e^-}$, which is nearly at rest in the laboratory,

$$p^\mu_\nu = p^\mu_{e^+e^-} - p^\mu_{observed}.$$

The errors made in this assumption are due to particles lost through inefficiency or limited acceptance, fake tracks and showers, and other undetected particles such as K_L^0 mesons, neutrons, or additional neutrinos. Several requirements are made to select events in which these effects are reduced and the neutrino four-momentum resolution is correspondingly enhanced.

Because extra neutrinos are correlated with extra leptons, events with an identified lepton in addition to the signal lepton are rejected. The primary source of fake tracks is from charged particles which do not have sufficient transverse momentum to reach the calorimeter and therefore curl in the tracking chambers, returning to the beam axis. The portions of the track after the initial outbound portion may be accidentally included as additional tracks. Criteria have been developed to identify such errors and make a best estimate of the actual charged particles in the event. Events for which the total charge of the tracks is not zero are removed, reducing the effect of lost or fake tracks. Showers in the calorimeter associated with tracks in the drift chamber are not used, so as not to double count their energy. A neural network algorithm has been developed to reject secondary hadronic showers associated with showers that are already associated with tracks.

A final neutrino reconstruction quality requirement is that the mass of the reconstructed neutrino to be small. The ratio of the reconstructed neutrino invariant mass squared, $M^2_{\rm miss}$, to twice the reconstructed neutrino energy is required to satisfy $|M^2_{\rm miss}/2E_\nu| < 0.35$ GeV$/c^4$. This quantity is proportional to the energy of a lost or fake particle. After this cut, the reconstructed neutrino's energy is assigned to be the magnitude of the missing momentum, because the momentum is not dependent on the particle identification of the tracks and so has a better resolution than the direct energy measurement.

Continuum events are suppressed by a combination of event shape and orientation criteria which exploit the fact that continuum events tend to be jet-like with a jet axis aligned with the beam axis, whereas $B\overline{B}$ events are more spherical and their orientation is uniformly distributed in the detector. The second Fox-Wolfram moment [8], R_2, of the energy flow in the event is required to be less than 0.4. In addition, a neural network is used to combine R_2, the angle between the lepton and the event thrust axis, the angle between the lepton momentum and the beam axis, and the fraction of the total energy lying in nine separate cones around the lepton direction, which cover the full the 4π solid angle. The R_2 cut is more than 99% and 95% efficient for $B \to X_c l\nu$ and $B \to X_u l\nu$, respectively, while removing 60% of the continuum events. The neural net cut removes an additional 73% of the continuum background, while keeping 92% and 94% of the $B \to X_c l\nu$ and $B \to X_u l\nu$, respectively.

After all cuts we observe 41411 events from CLEO II and 80440 events from CLEO II.V. The overall efficiency varies from 1.5% for $B \to X_c l\nu$ nonresonant to 4.2% for $B \to X_u l\nu$.

III. FIT TECHNIQUE

The full three-dimensional differential decay rate distribution as a function of the reconstructed quantities q^2, M_X^2, and $\cos\theta_{W\ell}$ is fit for the contributions from semileptonic B decay and backgrounds. The q^2 variable is replaced by $q^2/(E_\ell + E_\nu)^2$ for fitting purposes. The B decay modes are $B \to Dl\nu$, $B \to D^* l\nu$, $B \to D^{**} l\nu$, $B \to X_c l\nu$ nonresonant, and $B \to X_u l\nu$. The backgrounds are classified as secondary leptons, continuum leptons, or fake leptons. A secondary lepton is a real lepton in a $B\overline{B}$ event whose parent is not a B meson. A continuum lepton is a real lepton in a continuum $e^+e^- \to q\bar{q}$ event. A fake lepton is a non-leptonic track from either a $B\overline{B}$ or a continuum event which is identified as a lepton.

The normalization of the continuum lepton component is determined from the data taken below $B\overline{B}$ threshold. The normalization of the fake leptons is determined from the measured fake rates and the measured track spectra. The contributions of these two backgrounds are therefore not allowed to vary in the fit, while those of the secondary leptons and all of the $B \to Xl\nu$ modes are.

We perform a binned maximum-likelihood fit where component histograms are constructed from weighted Monte Carlo or data events. The fit uses electrons and muons simultaneously, with a separate set of histograms for each. The likelihood is implemented to take into account the histogram statistics using the method described in reference [9]. Projections of the Monte Carlo simulations of reconstructed quantities q^2, M_X^2, and $\cos\theta_{W\ell}$ for the various $B \to Xl\nu$ modes are shown in Figure 1. Projections of the data and fit result are shown in Figure 2.

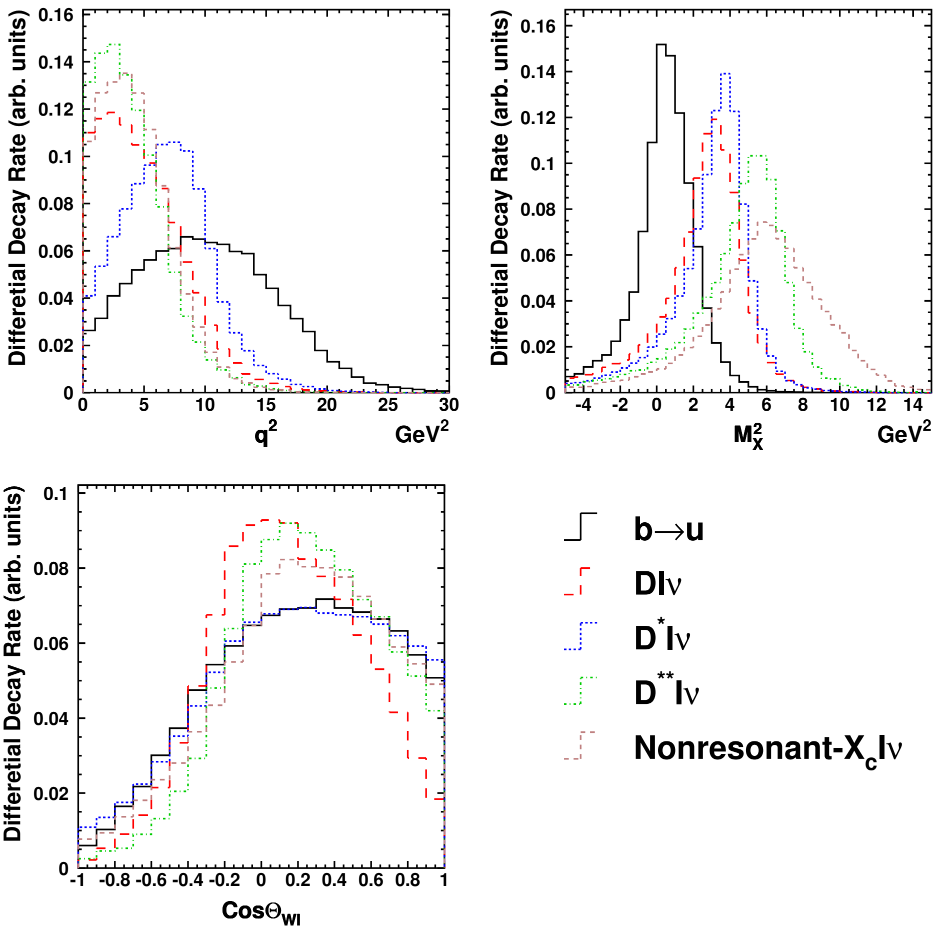

FIG. 1: Monte Carlo simulation of the distributions of the reconstructed quantities q^2, M_X^2, and $\cos\theta_{W\ell}$ for the various $B \to Xl\nu$ modes. The modes are $B \to X_u l\nu$ (solid), $B \to Dl\nu$ (short dash), $B \to D^* l\nu$ (dots), $B \to D^{**} l\nu$ (dot-dash), and $B \to X_c l\nu$ nonresonant (long dash). The curves are normalized to have unit area to facilitate comparison of the shapes. Note that due to finite resolution M_X^2 can be less than zero.

The $B \to Xl\nu$ modes, secondary leptons and real leptons from the continuum are modeled with events from a GEANT [7] simulation of the CLEO detector that are reconstructed in

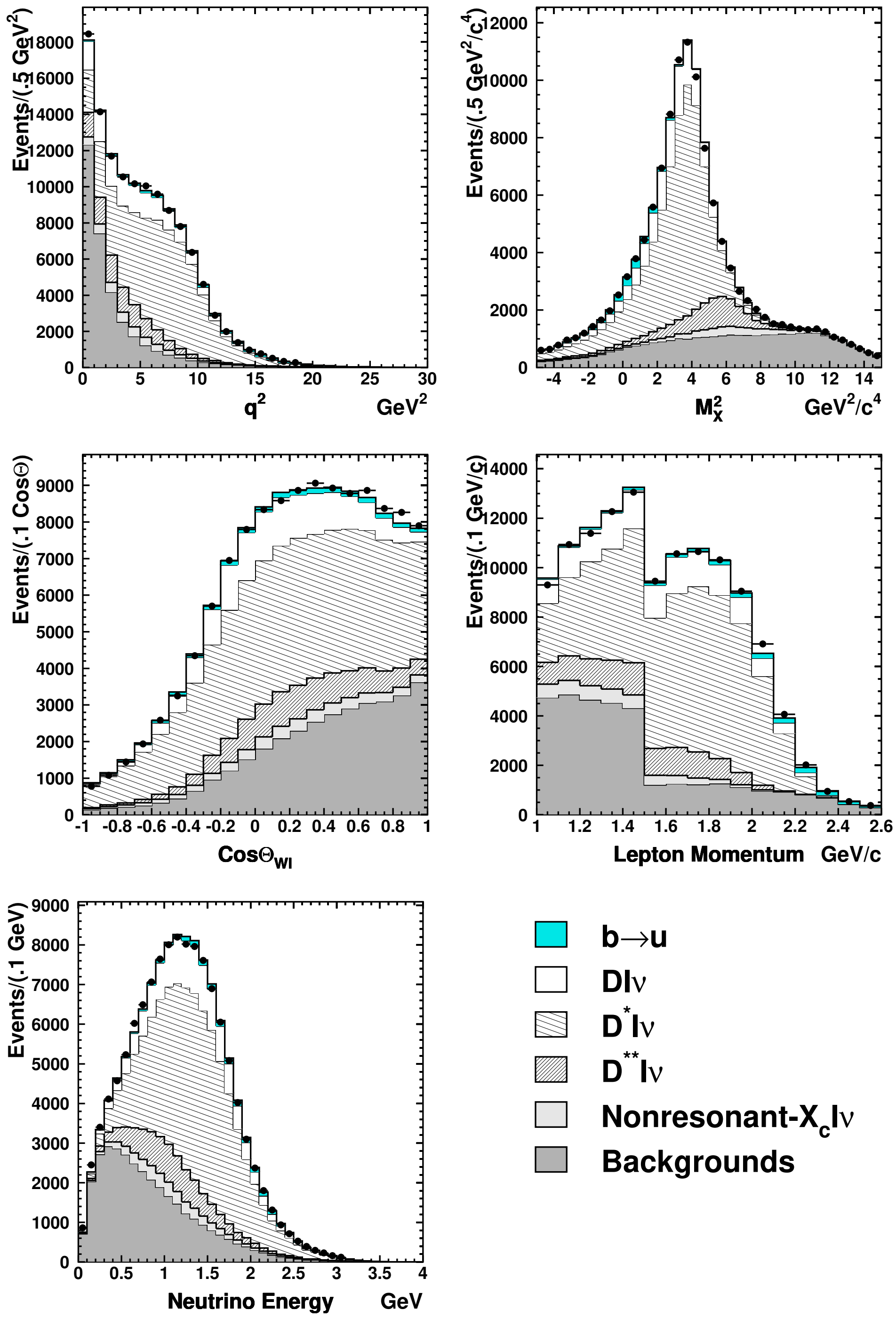

FIG. 2: Projections of the fit results in the reconstructed quantities, on the first row are q^2 and M_X^2, on the second are $\cos\theta_{W\ell}$ and E_ℓ, and on the third row is E_ν. From the top in each figure the histograms are the contributions from $B \to X_u l\nu$ (barely visible shaded), $B \to Dl\nu$ (open), $B \to D^* l\nu$ (sparsely hatched), $B \to D^{**} l\nu$ (densely hatched), $B \to X_c l\nu$ nonresonant (light shaded), and the sum of the backgrounds: continuum, secondary leptons, fake leptons (dark shaded). The step in the lepton momentum distribution is due to the looser muon identification used below 1.5 GeV/c for which there is a higher fake rate and higher efficiency.

the same manner as data events. The $B \to Dl\nu$ and $B \to D^*l\nu$ modes are simulated with HQET using the PDG [10] averages of measurements of the form factors. The $B \to D^{**}l\nu$ and $B \to X_u l\nu$ modes are simulated using form factors from the ISGW2 model [11]. The X_c nonresonant modes are simulated with the Goity and Roberts model [12] in which the D and D^* contributions are excluded.

The fake leptons are modeled with data events where a track is selected to be treated as a lepton. The events are then unfolded bin by bin to extract the π and K contributions, which are then multiplied by the measured fake rates. This models fake leptons from both $B\overline{B}$ and continuum. This method also provides an absolute normalization for the fake lepton contribution to the data sample. The real leptons from continuum are modeled with a Monte Carlo simulation which has been tuned to replicate the appropriate charm spectra; charm is the source of most leptons from continuum. The models of both continuum and fakes have been validated and constrained by comparisons with the 4.5 fb^{-1} of off-resonance data. The secondary leptons are modeled with CLEO's generic $B\overline{B}$ Monte Carlo which has also been tuned to replicate measured charm spectra and semileptonic charm decay measurements. To address the issue of the poorly understood charm counting in B decays, the charm counting in the $B\overline{B}$ Monte Carlo simulation is tuned to saturate the theoretically predicted level of charm production [13].

The $B \to Xl\nu$ models were varied to assess the dependence of the results on the model. The $B \to Dl\nu$ and $B \to D^*l\nu$ modes were varied within the range of the errors on the form factor measurements. The curvature of the form factors has not been measured and is usually constrained by theoretical predictions [14]. Because the data have an excess above the model in the q^2 region between 5.0 and 8.0 GeV$^2/c^4$, the curvature was set to 50% of its predicted value and varied by $\pm$50% of the prediction. The $B \to D^{**}l\nu$ form factor was replaced by a model inspired by HQET calculations [15]. The slope of the $B \to D^{**}l\nu$ and $B \to X_c l\nu$ nonresonant form factors in the q^2 dimension was also varied. The dominant model dependence is from the hadronic mass distribution of the $B \to X_c l\nu$ nonresonant mode. This is conservatively reweighted with a series of Gaussians restricted to the kinematically allowed region. The means of the Gaussians are allowed to range from $M_D + M_\pi$ to 3.5 GeV$/c^2$ with variances ranging from 0.25 GeV$^2/c^4$ to 1.25 GeV$^2/c^4$. The $B \to X_u l\nu$ simulation is varied from an all-nonresonant model to the nominal ISGW2 model [11], with a hybrid of the two in between. The all-nonresonant model differential decay rate corresponds to the prediction of HQET combined with CLEO's measurement of the $B \to X_s\gamma$ spectral function [16, 17]. The maximum deviation of the $B \to X_c l\nu$ nonresonant mass Gaussians is added in quadrature with the deviation of the other model variations to get the total model dependence.

Radiative corrections play an important role in the measurement of the M_X^2 distribution. The reconstructed M_X^2 is defined to be the mass squared of the system recoiling against the charged lepton and the neutrino. If a photon is radiated by the lepton in the event, it will be included in this definition of the recoil system,

$$M_X^2 = (p_B^\mu - p_\ell^\mu - p_\nu^\mu)^2 = (p_h^\mu + p_\gamma^\mu)^2. \tag{1}$$

The goal of this analysis is to measure the mass squared moment of the recoiling hadronic system p_h^2, not its combination with the radiated photon $(p_h + p_\gamma)^2$. To correct for this effect, the data are fit using fully simulated GEANT Monte Carlo events in which the PHOTOS package [18] has been used to generate radiated photons. The moments are calculated from the fit results and the theoretical models of the hadronic mass distributions for each mode and thus do not have a shift due to the radiative corrections.

However, knowledge of the radiative corrections is not complete. PHOTOS implements an algorithm based on a splitting function which applies the same physics at $\mathcal{O}(\alpha)$ as the prescription of Atwood and Marciano [19]. PHOTOS also includes a prescription for forcing the kinematics of the decay to conserve momentum in addition to energy. The implementation of PHOTOS has been checked in detail against a private implementation of the same algorithm. The applicability of the PHOTOS algorithm is however not exact. The calculation ignores the internal structure of the hadronic system. Richter-Wąs [20] has made a comparison of the PHOTOS and Atwood-Marciano prescriptions with an exact order-α calculation of the radiative corrections to the $B^- \to D^0\ell^-\overline{\nu}$ differential decay rate and has found agreement at the 20% and 30% level, respectively. Because we must extrapolate to the other $B \to X_c l\nu$ modes, we make a conservative estimate that the PHOTOS calculation can be trusted to $\pm 50\%$.

The application of the radiative corrections is further complicated by the fact that the generated photons are low energy and often lost. When the photon is lost it can cause the event to fail the missing mass cut. If the event does pass the missing mass cut, the reconstructed neutrino will be biased toward high energy, pushing the reconstructed M_X^2 toward the true hadronic mass squared without the photon. If neglected, this would increase the measured $\langle M_X^2 - \overline{M}_D^2\rangle$ moment with a 1.0 GeV lepton energy cut by 0.082 GeV$^2/c^4$, before detector effects are included. This would be reduced to 0.037 GeV$^2/c^4$ after detector effects.

The method of neutrino reconstruction adds a large amount of kinematic information to each event. However, it also adds significant potential for systematic errors. The resolution on the neutrino kinematics is affected by the models of the signal, the other B in the event, and the detector response. The GEANT Monte Carlo simulation does not perfectly reproduce the track and shower efficiencies and fake rates, nor are B decays well enough understood that the inclusive particle distributions are well known. For this analysis we employ a reweighting method in order to quantify the effects of these uncertainties on our results. For example, to study the effect of the tracking efficiency uncertainty, the Monte Carlo events in which tracks are lost are given a higher or lower weight in constructing the component histograms for the fit. The scale of the variation can in general be constrained by direct measurements of the quantity being varied. One important example is that having a K_L^0 in the event adds a tail to the neutrino resolution. The inclusive K_S^0 spectrum in $B\overline{B}$ events has been measured and can be used to constrain the K_L^0 spectrum. The dominant detector systematics are fake showers (generally splitoffs from hadronic showers), final state radiation, and fake leptons. The detector systematics are summed in quadrature to arrive at the overall detector systematic error.

IV. RESULTS

The fit results can be used to calculate a branching fraction for each of the hadronic final states $B \to Dl\nu$, $B \to D^*l\nu$, $B \to D^{**}l\nu$, and $B \to X_c l\nu$ nonresonant. From these branching fractions the moment $\langle M_X^2 - \overline{M}_D^2\rangle$ with a certain lepton energy cut can be calculated as follows:

$$\langle M_X^2 - \overline{M}_D^2\rangle_{cut} = \frac{\sum_m m_m c_m \mathcal{B}_m}{\sum_m c_m \mathcal{B}_m}, \tag{2}$$

where m_m is the moment of mode m with the cut applied, c_m is the fraction of mode m passing the cut, and $\mathcal{B}_m$ is the branching fraction of mode m. The quantities m_m and c_m depend only on the model. The measured branching fractions, $\mathcal{B}_m$, depend on the model, the detector simulation, and the data.

For each lepton energy cut, the fit is repeated with the cut applied using the reconstructed (lab frame) quantity. Theoretical calculations of $\langle M_X^2 - \overline{M}_D^2\rangle$, however, are made with the cut in the B rest frame [5, 21]. The moments reported are therefore calculated in the B rest frame. This involves a small extrapolation.

The resulting moments are shown in Table I. These moments are highly correlated because they share some fraction of the data and also use the same models and detector simulation. The statistical correlations are assessed with a simple Monte Carlo simulation. The model dependence and detector systematic correlations are assessed by summing the covariance matrices from each systematic error. The resulting covariance matrix is shown in Table II. An alternative representation of the data is to use the $\langle M_X^2 - \overline{M}_D^2\rangle$ moment with a 1.5 GeV lepton energy cut and the difference between the $\langle M_X^2 - \overline{M}_D^2\rangle$ moments at 1.0 and 1.5 GeV. These two measurements are significantly less correlated. We find

$$\langle M_X^2\rangle_{E_\ell>1.0\,\mathrm{GeV}} - \langle M_X^2\rangle_{E_\ell>1.5\,\mathrm{GeV}} = (0.163 \pm 0.014 \pm 0.036 \pm 0.064)\,\mathrm{GeV}^2/c^4$$

and a covariance of this value with the $\langle M_X^2 - \overline{M}_D^2\rangle_{E_\ell>1.5\,\mathrm{GeV}}$ moment of $2.242\times10^{-3}\,\mathrm{GeV}^4/c^8$.

TABLE I: $\langle M_X^2 - \overline{M}_D^2\rangle$ versus the lepton energy cut. The errors on the entries in the table are the statistical, detector systematics, and model dependence, respectively.

Cut (GeV)	$\langle M_X^2 - \overline{M}_D^2\rangle$ (GeV$^2/c^4$)
$E_\ell > 1.0$	$0.456 \pm 0.014 \pm 0.045 \pm 0.109$
$E_\ell > 1.1$	$0.422 \pm 0.014 \pm 0.031 \pm 0.084$
$E_\ell > 1.2$	$0.393 \pm 0.013 \pm 0.027 \pm 0.069$
$E_\ell > 1.3$	$0.364 \pm 0.013 \pm 0.030 \pm 0.054$
$E_\ell > 1.4$	$0.332 \pm 0.012 \pm 0.027 \pm 0.055$
$E_\ell > 1.5$	$0.293 \pm 0.012 \pm 0.033 \pm 0.048$

TABLE II: Covariance of $\langle M_X^2 - \overline{M}_D^2\rangle$ moments with different lepton energy cut. The rows/columns correspond to progressively more restrictive lepton energy cut starting with 1.0 GeV and ending with 1.5 GeV.

$$\begin{pmatrix} 1.421 & 1.096 & 0.913 & 0.724 & 0.735 & 0.618 \\ 1.096 & 0.864 & 0.719 & 0.577 & 0.574 & 0.486 \\ 0.913 & 0.719 & 0.612 & 0.495 & 0.499 & 0.422 \\ 0.724 & 0.577 & 0.495 & 0.413 & 0.418 & 0.352 \\ 0.735 & 0.574 & 0.499 & 0.418 & 0.447 & 0.373 \\ 0.618 & 0.486 & 0.422 & 0.352 & 0.373 & 0.324 \end{pmatrix} \times 10^{-2}\ \mathrm{GeV}^4/c^8$$

Figure 3 shows a comparison of the results with previous measurements [2, 3] and a prediction based on HQET constrained by this measurement of $\langle M_X^2 - \overline{M}_D^2\rangle_{E_\ell>1.5}$ and the first $B \to X_s\gamma$ photon energy moment [17]. The results agree well with both. The theory bands shown in the figure reflect the experimental errors on the two constraints, the variation of the third-order HQET parameters by the scale (0.5 GeV)^3, and variation of the size of the higher order QCD radiative corrections [21].

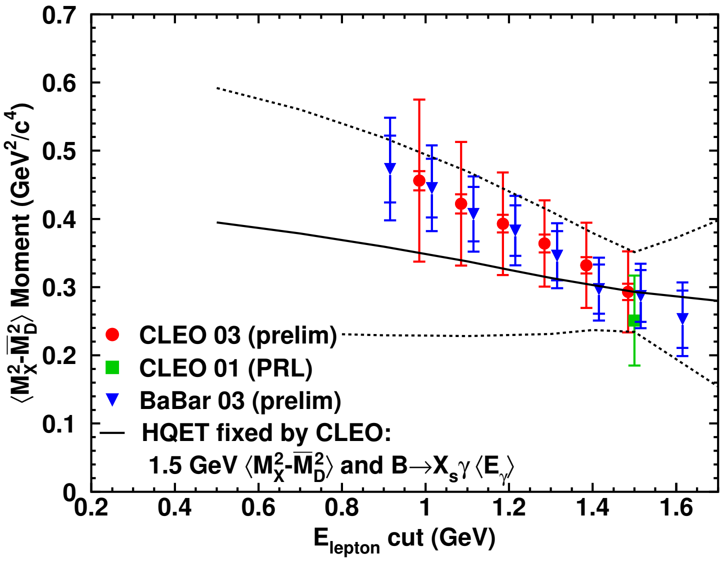

FIG. 3: The results of this analysis compared to previous measurements [2, 3] and the HQET prediction. The theory bands shown in the figure reflect the variation of the experimental errors on the two constraints, the variation of the third-order HQET parameters by the scale (0.5 GeV)^3, and variation of the size of the higher order QCD radiative corrections [21].

V. CONCLUSION

We have measured the moment $\langle M_X^2 - \overline{M}_D^2\rangle$ as a function of the lepton energy cut with a minimum cut of 1.0 GeV. We obtain the preliminary result,

$$\langle M_X^2 - \overline{M}_D^2\rangle_{E_\ell > 1.0\,\mathrm{GeV}} = (0.456 \pm 0.014 \pm 0.045 \pm 0.109)\ \mathrm{GeV}^2/c^4.$$

This result provides a test of the HQET predictions using a larger portion of the available decay rate. We have also improved the precision of the measurement with a 1.5 GeV lepton energy cut, obtaining the preliminary result

$$\langle M_X^2 - \overline{M}_D^2\rangle_{E_\ell > 1.5\,\mathrm{GeV}} = (0.293 \pm 0.012 \pm 0.033 \pm 0.048)\ \mathrm{GeV}^2/c^4.$$

Measurements such as these can be used to improve the determination of the Standard Model parameter $|V_{cb}|$. They also provide a valuable test of the HQET inclusive predictions which are used in the extraction of $|V_{ub}|$ and $|V_{cb}|$ and in the interpretation $B \to X_s\gamma$.

We gratefully acknowledge the contributions of the CESR staff for providing the luminosity and the National Science Foundation and U.S. Department of Energy for supporting this research.

---

[1] J. Chay, H. Georgi and B. Grinstein, Phys. Lett. B **247**, 399 (1990); I. I. Bigi, M. A. Shifman, N. G. Uraltsev and A. I. Vainshtein, Phys. Rev. Lett. **71**, 496 (1993) [arXiv:hep-ph/9304225]; A. V. Manohar and M. B. Wise, Phys. Rev. D **49**, 1310 (1994).

[2] S. E. Roberts, PhD thesis, University of Rochester, UMI-98-08907; D. Cronin-Hennessy *et al.* [CLEO Collaboration], Phys. Rev. Lett. **87**, 251808 (2001) [arXiv:hep-ex/0108033].

[3] B. Aubert, *et al.* [BaBar Collaboration], hep-ex/0307046.

[4] J. P. Alexander *et al.* [CLEO Collaboration], Phys. Rev. Lett. **77**, 5000 (1996).

[5] A. F. Falk and M. E. Luke, Phys. Rev. D **57**, 424 (1998) [arXiv:hep-ph/9708327].

[6] Y. Kubota *et al.*, Nucl. Instrum. Meth. A **320**, 66 (1992); T. S. Hill, Nucl. Instrum. Meth. A **418**, 32 (1998).

[7] R. Brun *et al.*, GEANT 3.15, CERN Report No. DD/EE/84-1 (1987).

[8] G. C. Fox and S. Wolfram, Phys. Rev. Lett. **41**, 1581 (1978).

[9] R. J. Barlow and C. Beeston, Comput. Phys. Commun. **77**, 219 (1993).

[10] K. Hagiwara *et al.* [Particle Data Group Collaboration], Phys. Rev. D **66**, 010001 (2002).

[11] D. Scora and N. Isgur, Phys. Rev. D **52**, 2783 (1995) [arXiv:hep-ph/9503486].

[12] J. L. Goity and W. Roberts, Phys. Rev. D **51**, 3459 (1995) [arXiv:hep-ph/9406236].

[13] C. Caso *et al.* [Particle Data Group Collaboration], Eur. Phys. J. C **3**, 1 (1998).

[14] C. G. Boyd, B. Grinstein and R. F. Lebed, Phys. Lett. B **353**, 306 (1995) [arXiv:hep-ph/9504235]; I. Caprini and M. Neubert, Phys. Lett. B **380**, 376 (1996) [arXiv:hep-ph/9603414]; C. G. Boyd, B. Grinstein and R. F. Lebed, Phys. Rev. D **56**, 6895 (1997) [arXiv:hep-ph/9705252]; I. Caprini, L. Lellouch and M. Neubert, Nucl. Phys. B **530**, 153 (1998) [arXiv:hep-ph/9712417].

[15] A. K. Leibovich, Z. Ligeti, I. W. Stewart and M. B. Wise, Phys. Rev. D **57**, 308 (1998) [arXiv:hep-ph/9705467].

[16] M. Neubert, Phys. Rev. D **49**, 3392 (1994) [arXiv:hep-ph/9311325]; M. Neubert, Phys. Rev. D **49**, 4623 (1994) [arXiv:hep-ph/9312311]; I. I. Bigi, M. A. Shifman, N. Uraltsev and A. I. Vainshtein, Phys. Lett. B **328**, 431 (1994) [arXiv:hep-ph/9402225]; A. L. Kagan and M. Neubert, Eur. Phys. J. C **7**, 5 (1999) [arXiv:hep-ph/9805303]; F. De Fazio and M. Neubert, JHEP **9906**, 017 (1999) [arXiv:hep-ph/9905351]; A. K. Leibovich, I. Low and I. Z. Rothstein, Phys. Rev. D **61**, 053006 (2000) [arXiv:hep-ph/9909404].

[17] S. Chen *et al.* [CLEO Collaboration], Phys. Rev. Lett. **87**, 251807 (2001) [arXiv:hep-ex/0108032].

[18] E. Barberio and Z. Wąs, Comput. Phys. Commun. **79**, 291 (1994).

[19] D. Atwood and W. J. Marciano, Phys. Rev. D **41**, 1736 (1990).

[20] E. Richter-Wąs, Phys. Lett. B **303**, 163 (1993).

[21] C. W. Bauer, Z. Ligeti, M. Luke and A. V. Manohar, Phys. Rev. D **67**, 054012 (2003) [arXiv:hep-ph/0210027].